HHS Public Access

Author manuscript

Oncogene. Author manuscript; available in PMC 2019 June 05.

Published in final edited form as:

Oncogene. 2019 March ; 38(13): 2380–2393. doi:10.1038/s41388-018-0581-9.

Cisplatin-induced immune modulation in ovarian cancer mouse models with distinct inflammation profiles

Shannon Grabosch[#1,2,3], **Mirna Bulatovic**[#1,2], **Feitianzhi Zeng**[1,2,4], **Tianzhou Ma**[5], **Lixin Zhang**[1,2], **Malcolm Ross**[1,2,3], **Joan Brozick**[1], **YuSi Fang**[5], **George Tseng**[5], **Eun Kim**[6], **Andrea Gambotto**[5], **Esther Elishaev**[7], **Robert. P Edwards**[1,2,3], and **Anda M. Vlad**[1,2]

[1]Magee Womens Research Institute, Pittsburgh, Pennsylvania, United States of America

[2]Department of Obstetrics, Gynecology and Reproductive Sciences, University of Pittsburgh School of Medicine, Pittsburgh, Pennsylvania, United States of America

[3]Magee Womens Hospital of the University of Pittsburgh Medical Center, Pittsburgh, Pennsylvania, United States of America

[4]Central South University Xiangya School of Medicine, Changsha, Hunan, People's Republic of China

[5]Department of Biostatistics, University of Pittsburgh Graduate School of Public Health, Pittsburgh, Pennsylvania, United States of America

[6]Department of Surgery, University of Pittsburgh School of Medicine, Pittsburgh, Pennsylvania, United States of America

[7]Department of Pathology, University of Pittsburgh School of Medicine, Pittsburgh, Pennsylvania, United States of America

[#] These authors contributed equally to this work.

Abstract

The backbone of ovarian cancer treatment is platinum-based chemotherapy and aggressive surgical debulking. New therapeutic approaches using immunotherapy via immune checkpoint blockade, which have demonstrated clinical efficacy in other tumor types, have been less promising in ovarian cancer. To increase their clinical efficacy, checkpoint inhibitors are now being tested in clinical trials in combination with chemotherapy.

Here, we evaluated the impact of cisplatin on tumor immunogenicity and its in vivo roles when used alone or in combination with anti-PD-L1, in two novel murine ovarian cancer cell models.

Corresponding author Anda M. Vlad, MD PhD, Department of Obstetrics, Gynecology and Reproductive Sciences, University of Pittsburgh, School of Medicine, Magee-Womens Research Institute B403, 204 Craft Ave, Pittsburgh PA 15213, Tel: 412 641 2985; Fax: 412 641 6156, vladam@upmc.edu.

Conflict of Interests

Authors have no conflict of interest.

Data Availability

The datasets generated during and/or analysed during the current study are available from the corresponding author on reasonable request.

The 2F8 and its platinum-resistant derivative 2F8cis model, display distinct inflammatory profiles and chemotherapy sensitivities, and mirror the primary and recurrent human disease, respectively. Acute and chronic exposure to cisplatin enhances tumor immunogenicity by increasing calreticulin, MHC class I, antigen presentation and T cell infiltration. Cisplatin also upregulates PD-L1 expression in vitro and in vivo, demonstrating a dual, paradoxical immune modulatory effect and supporting the rationale for combination with immune checkpoint blockade. One of the pathways activated by cisplatin treatment is the cGAS/STING pathway. Chronic cisplatin treatment led to upregulation of cGAS and STING proteins in 2F8cis compared to parental 2F8 cells, while acute exposure to cisplatin further increases cGAS and STING levels in both 2F8 and 2F8cis cells. Overexpression of cGAS/STING modifies tumor immunogenicity by upregulating PD-L1, MHC I and calreticulin in tumor cells. Anti-PD-L1 alone in a platinum-sensitive model or with cisplatin in a platinum-resistant model increases survival. These studies have high translational potential in ovarian cancer.

Keywords

Ovarian cancer; cisplatin; PD-L1; immunotherapy; inflammation; STING; mouse models

Introduction

Epithelial ovarian cancer (EOC) is a lethal diagnosis within 5 years, for over half of the 22,000 women diagnosed annually in the United States [1]. Despite the gold standard of aggressive surgical debulking and platinum-based chemotherapy resulting in initial response rates as high as 80% [2], most women experience tumor recurrence and ultimately succumb to chemoresistant disease. Overall survival rates have remained largely unchanged since the introduction of cisplatin more than four decades ago, raising the need for new and improved therapeutic approaches [3]. Immunotherapy of solid tumors has experienced remarkable progress in recent years, primarily driven by the success seen with immune checkpoint blockade in melanoma, lung, urothelial and head and neck cancers [4–7]. Emerging results from early stage clinical trials suggest that the beneficial effect of immune therapies could also extend to a subset of EOC patients [8, 9].

Studies from Hamanishi et al, were the first to demonstrate a benefit of PD-1/PD-L1 blockade in EOC [10, 11], providing a rationale for further investigation of immune checkpoint blocking antibodies, including nivolumab (anti-PD-1), pembrolizumab (anti-PD-1) and avelumab (anti-PD-L1) [11–13]. To increase clinical efficacy, several ongoing studies aim to establish the benefit of administering checkpoint inhibitors as part of combinatorial approaches, in primary and recurrent disease [14]. Additional efforts focus on the identification of biomarkers predictive of response to immune checkpoint blockade, which could be applied for pre-treatment selection. Some of the biomarkers currently under investigation focus on the cellular and molecular characteristics of the tumor immune microenvironment.

Evidence from non-ovarian cancer types shows that patients with immunogenic, T cell infiltrated “hot” tumors show durable clinical benefit in response to PD-1/PD-L1 blockade,

in contrast to patients with non-immunogenic ("cold") tumors [15]. In EOC, most tumors show signs of moderate to high T cell infiltration and successful development of new immune therapeutic strategies depends in part on the advent of preclinical models that adequately model these T cell inflammation patterns. We have recently developed two new in vivo syngeneic mouse models with different inflammatory profiles and different susceptibilities to cisplatin. Cisplatin, commonly used in EOC, is a chemotherapy drug that kills cancer cells by crosslinking DNA and inhibiting mitosis [16]. The original dogma stating that chemotherapy negatively impacts anti-tumor immunity in the host has been challenged in recent years, by studies showing that some anti-neoplastic drugs can in fact act as a pro-inflammatory stimulus [17–20]. We postulate that cisplatin promotes immune recognition and immune-mediated tumor elimination. Our studies measured the cisplatin-induced effects on tumor immunogenicity in vitro and in vivo and tested the in vivo therapeutic effect of cisplatin and anti-PD-L1 either alone or in combination. Using tumors with moderate and high T cell infiltration we show that cisplatin upregulates a DNA recognition pathway, induces genes involved in antigen processing and presentation and augments T cell infiltration. Cisplatin also induces PD-L1 in tumor cells, suggesting dichotomous roles and supporting the need for combination with PD-1/PD-L1 blockade. These preclinical studies in novel mouse models have translational significance for future development of combination therapies in ovarian cancer.

Results

Cisplatin induces PD-L1 up-regulation in human and mouse ovarian cancer cell lines in vitro and in vivo

We tested the effect of cisplatin on PD-L1 expression in human ovarian cancer cell lines that mirror the drug susceptibility seen in patients, especially at the time of diagnosis (cisplatin-sensitive primary disease) or at first or second recurrences with increased drug resistance. (Fig. 1A). Exposure of high grade serous ovarian tumor-derived OVCA420 and OVCA432 cells [21, 22] to IC50 cisplatin triggers PD-L1 upregulation in a time-dependent manner (Fig. 1B-G and Suppl. Fig 1) and a similar, at least five-fold increase in the frequency of positive cells was seen in both lines, with an earlier kinetics in the cisplatin resistant OVCA420 cellsTreatment-induced increase in the whole PD-L1 protein expression, measured in the cell lysate by Western blot (Fig. 1D and G), correlated with the increase in the cell surface fraction, captured by flow cytometry (Fig. 1B and E).

To model platinum resistance in immune competent mice, we generated 2F8cis cells, which represent the cisplatin-resistant derivative of parental 2F8 cells. The 2F8 cells represent a monoclonal cancer cell population derived from a de novo, orthotopic mouse ovarian tumor [23, 24]. Through repeated, long-term exposure of 2F8 cells to increasing concentration of cisplatin and more than 180 days of in vitro propagation, the cells acquired moderate cisplatin resistance (IC50 of 2.5 μM for 2F8 versus 11.8 μM for 2F8cis cells) (Fig. 2A). Chronic treatment with cisplatin stimulated PD-L1 expression in 2F8cis cells and acute in vitro exposure to IC50 cisplatin further increases PD-L1 levels in both 2F8 and 2F8cis cells (Fig. 2B). PDL1 upregulation was also observed in response to other chemotherapeutic drugs, such as carboplatin, gemcitabine and doxorubicin.The PD-L1- inducing effect of all

drugs was most prominent in the cisplatin-resistant OVCA420 and 2F8cis cells. Gemcitabine also upregulated PDL1 in 2F8 cells (Suppl Fig. 2).

To monitor the effect of cisplatin on PD-L1 expression in vivo, we injected the 2F8 and 2F8cis cells in syngeneic, immune competent female mice. Intraperitoneal (IP) injection of 2F8 and 2F8cis cells triggers numerous, high grade tumor implants with undifferentiated histology. The tumors grow aggressively, including in the upper abdomen, mirroring the peritoneal carcinomatosis often seen in late stage EOC (Fig. 2C, F). Tissue PD-L1 expression is lower in 2F8 compared to 2F8cis tumors (Fig. 2D, G) but increases following two rounds of in vivo cisplatin treatment (Fig. 2E, H), in line with in vitro results.

Cisplatin boosts tumor immunogenicity

Although 2F8 and 2F8cis peritoneal tumor implants have a similar in vivo distribution pattern, the tumors show distinct inflammation profiles. The 2F8 tumors have low/moderate T cell infiltration (Fig. 2I) consistent with the phenotype of “warm” tumors. In contrast, the 2F8cis tumors show significantly higher CD8 T cell infiltration, indicating an immunological “hot” phenotype (Fig. 2K, L). T cells were often seen as conglomerates within the 2F8cis tumors (Fig. 2N). The conglomerates resemble tertiary lymphoid structures (TLS), occasionally reported in various solid tumor types [25]. The presence of TLS was significantly higher in 2F8cis (17 out of 32 mice) versus 2F8 tumor bearing mice (1 out of 24 mice, $p< 0.0001$, Fisher’s exact). Overall, these low and high T cell infiltration patterns in 2F8 and 2F8cis tumors respectively, correlate with tissue PD-L1 expression, as also reported in other tumor types [26]. Furthermore, we observed that, like the effect on PD-L1 expression, in vivo exposure to cisplatin further increased T cell infiltration in 2F8 tumors, facilitating the transition from a “warm” to a “hot” immune phenotype (Fig. 2J).

To explore the mechanisms responsible for the differences in baseline immunogenicity of “warm” 2F8 and “hot” 2F8cis tumors, and to identify how cisplatin changes tumor inflammation, we performed RNAseq on 2F8 and 2F8cis cells, with and without in vitro cisplatin treatment. As reference, we used cells exposed to IFNα, a potent inducer of immune modulatory genes, including PD-L1[27] (Suppl. Fig. 3).

We profiled the single nucleotide variants (SNVs) of untreated 2F8 and 2F8cis cells, using as reference the whole exome of healthy mouse ovarian surface epithelial cells from syngeneic mice, and identified 5145 and 5272 gene variants, respectively. Of these, 4495 SNVs were common to both cell lines and 29% of all variants were non-synonymous.

When comparing the 2F8cis cells against the parental 2F8 cells, we identified 202 variants that are specific to the 2F8cis cells. Importantly, most (77%) of these cisplatin-induced SNVs are non-synonymous and located across the entire exome (Fig. 3A and Suppl. Table 1). These results demonstrate that chronic exposure to cisplatin led to increased rate of accumulation of non-synonymous mutations, which may increase the potential for neoepitope presentation, and subsequent T cell immune reactivity [28].

Differentially expressed (DE) genes upregulated by acute exposure to cisplatin or IFNα in 2F8 and 2F8cis cells are shown in Fig. 3B and listed in Suppl. Table 2. Of all cisplatin-

triggered genes in both 2F8 and 2F8cis cells (n=352 DE genes), 51 genes (14%) were also induced by IFNα (Suppl. Table 2), demonstrating a partial overlap between the cisplatin-induced and proinflammatory, IFNα-induced effects (Fig. 3C). Pathway analyses show that the overlapping genes are important for several immunogenic pathways, like activation of innate immunity via DNA-dependent activators of IFN regulatory factors (*Irf7, Ifih1, Zbp1*), antigen presentation pathways (*Tap1, Tap2, MHC class I*), and "eat-me" signals like calreticulin (*Calr*) [29] etc. (Fig. 3D and Suppl. Table 2).

We confirmed that cisplatin treatment increases MHC I cell surface expression in 2F8 and 2F8cis cells, which could augment antigen presentation and the potential for CD8 T cell recognition (Fig. 3E). We note that 2F8 cells have lower baseline MHC I expression, partly explaining the lower immune infiltration seen in vivo in the 2F8 compared to the "hot", immune reactive 2F8cis tumors. In line with the RNAseq data, in vitro exposure to cisplatin triggers upregulation and translocation at the plasma membrane of calreticulin, in both cell lines (Fig. 3F). Overall, these results suggest that exposure to cisplatin has dual potential: it can increase tumor immunogenicity by triggering non-synonymous mutations, boosting antigen presentation and accumulation of tumor infiltrating lymphocytes (TIL), while also altering immune evasion through PD-L1 upregulation.

Cisplatin triggers cGAS/STING

To identify potential mechanisms by which cisplatin contributes to the tumor-immune cell interface, we focused on the overlapped DE genes, upregulated by both cisplatin and IFNα (Fig. 3C and D). Pathway analysis shows that the most dysregulated pathway comprising the overlapped genes involves the activation of interferon regulatory factors by cytosolic pattern recognition receptors. Given that cisplatin is a DNA damage-inducing drug, we interrogated the cyclic GMP-AMP synthase (cGAS), a DNA sensor, and its direct target, the stimulator of interferon genes (STING). The cGAS/STING pathway is a DNA sensing pathway normally involved in sensing cytosolic DNA primarily post-viral infections. As more recently recognized, this pathway can also be triggered by antineoplastic, DNA damage inducing agents [30].

The 2F8cis cells, which have been generated via repeated long-term exposure to cisplatin, and express higher baseline PD-L1 (Fig. 2) also express higher cGAS and STING protein levels compared to 2F8 cells in vitro (Fig. 4A), and in vivo (Fig. 4B), confirming the RNAseq gene expression results (Suppl. Table 3). Acute exposure to cisplatin further increases cGAS and STING levels in both 2F8 and 2F8cis cells (Fig. 4A and Supplem. Fig 4). To test whether direct engagement of the cGAS/STING pathway modulates tumor PD-L1 expression, we treated PD-L1^{low} 2F8 cells with direct STING agonists 2'3'- cyclic guanosine monophosphate–adenosine monophosphate (cGAMP) and interferon stimulatory DNA (ISD). Both treatments increased PD-L1 levels, compared to control-treated cells (Fig. 4C). The effect on PD-L1 can be seen early (6 h) following exposure to 2'3- cGAMP, whereas PD-L1 upregulation due to ISD follows a slower kinetics, with largest increase seen at 48 h. Treatment also increases MHC I expression, peaking at 48 h for both drugs (Fig. 4D).

To test whether overexpression of cGAS/STING changes PD-L1 expression, we exposed the PD-L1^{low} cGAS/STING^{low} 2F8 cells to either a cGAS/STING- encoding adenovirus (Ad5.cGAS/STING) or control adenovirus (Ad5.EGFP). The efficiency of infection was 86%. As expected, control adenovirus also triggers significant PD-L1 expression (in response to viral DNA), with 46% of cells expressing PD-L1. However, virtually all tumor cells became PD-L1 positive when exposed to Ad5.GAS/STING (Fig. 4E). Similarly, transfection of MHC I^{low} 2F8 cells with Ad5.GAS/STING renders virtually all cells MHC I^{high}. These results demonstrate that, similarly to the effects of cisplatin, direct activation of the cGAS/STING can boost tumor immunogenicity by increasing MHC I expression. Additionally, the pathway can also lead to adaptive immune resistance through PD-L1 upregulation.

Combination chemo-immune therapy increases survival in moderately resistant 2F8cis tumors

To explore in vivo the therapeutic efficacy of cisplatin in combination with PD-1/PD-L1 blockade, we challenged the mice IP with 2F8 and 2F8cis cells. For each tumor model, four groups of mice were enrolled, receiving either IP cisplatin, IP anti-PD-L1 or combination cisplatin/anti-PD-L1. Control mice received IP rat IgG and IP PBS.

In the cisplatin-sensitive, “warm” 2F8 model, survival was increased by single agent cisplatin and anti-PD-L1, respectively (Fig. 5A). Anti-PD-L1 significantly decreased tumor weight, triggered tissue necrosis and increased Foxp3 TILs (Fig. 5B-E). Cisplatin alone or in combination increased CD8 T cell accumulation. Although 20% of mice treated with combination therapy were alive at the end of protocol, the overall survival response was not significantly higher compared to control mice (Fig. 5A). No signs of nephrotoxicity were observed in the combination group, with creatinine and blood urea nitrogen (measurements of kidney function) being within normal ranges.

In the inflamed 2F8cis model, 30% of mice treated with anti-PDL1 alone survived at the end of protocol, although a significant increase was seen only in the combination therapy group (Fig. 5A). No significant changes in tissue necrosis or T cell infiltration were observed in any of the treatment groups for the 2F8cis model (Fig. 5C-E).

To further identify treatment-induced changes in the tumor immune microenvironment, we performed NanoString analyses, using a collection of n=751 immune genes, with known functions in anti-tumor immunity and tumor inflammation. All DE genes from comparisons of treatments versus control, for each tumor model are presented in Suppl. Table 4.

The heatmaps in Fig. 5F show the relative expression of DE immune genes triggered by PD-L1 and cisplatin treatment, both of which reduced tumor burden and increased survival in 2F8 tumors, compared to control animals. Anti-PD-L1 increased expression of genes encoding for all major T cell markers (CD3, CD4, CD8), cytotoxic effector molecules and activation markers (granzymes, perforin, ICOS), IFNγ and IFNγ-induced genes including T cell attracting chemokines (CXCL-9, −10–11) (Suppl. Table 4 and 5).

In the cisplatin group, the clear majority (89%) of the cisplatin-induced DE immune genes were similarly upregulated by immunotherapy with anti-PD-L1, further demonstrating the immune modulatory roles of cisplatin. Despite low expression in 2F8 cells, STING (*Tmem173*), MHC I (*H2-Kb*) and TAP1 (*Tap1*) gene expression changed significantly with in vivo treatment ($p<0.05$, ANOVA, Suppl. Table 4), in line with findings from our in vitro experiments (Fig. 4).

NanoString gene expression profiling of control-treated 2F8cis versus control-treated 2F8 tumors demonstrate increased expression of CCL5 (RANTES, Suppl. Table 6), a chemotactic T cell factor, which may explain the increased T cell infiltration seen in the 2F8cis model (Fig. 2). However, the 2F8cis tumors also show increased expression of *Tgfβ, Stat3 and B7-H3* (Suppl. Table 6) which, together with evidence on regulatory T cell infiltration, suggests an immune suppressive environment in 2F8cis tumors.

Immune gene fluctuations induced by the cisplatin/anti-PDL1 combination treatment in 2F8cis tumors were more modest (n=16 DE genes, Fig. 5G and Suppl. Table 4). However, eight of the 16 DE genes triggered by cisplatin/PD-L1 in 2F8cis cells were also significantly changed by the two survival-inducing treatments in the 2F8 tumor model. Notably, some of these genes like the proteasome subunit beta types 9, (*Psmb9,* encoding for LMP2) and *Psbmb10* (encoding for LMP10), are IFNγ regulated genes in the antigen processing and presentation machinery and play important roles in the immune recognition of target cells alongside TAP1/TAP2 and MHC I. These results highlight the immune modulatory roles of cisplatin when used in vivo, alongside immune checkpoint blockade in tumors with various response to cisplatin.

Discussion

In contrast to the long-held belief that cisplatin is immunosuppressive, more recent evidence indicates that the anticancer activity of cisplatin may also be related to its ability to act as an immune modulator [17–20]. However, the mechanisms by which cisplatin modulates the immune microenvironment in ovarian cancer are not fully understood. Using novel preclinical EOC models with different cisplatin susceptibilities and unique inflammation profiles, we show that chronic and acute exposure to cisplatin promotes intra-tumoral T cell accumulation, increases immunogenicity of the cancer cells and leads to upregulation of immunogenic cell markers (calreticulin), MHC I, and molecules in the antigen processing and presentation pathway (Tap1/2, Lamp2/10). Combined with the fact that cisplatin increases the tumor mutational load and the potential for neo-epitope formation, these findings provide the rationale for future exploration of neoantigen vaccines in recurrent, immunogenic tumors. Nevertheless, cisplatin treatment seems to have a dual effect, since both acute and chronic exposure to cisplatin triggers upregulation of tumor PD-L1, pointing to the need for combination with immune checkpoint blockade.

One potential mechanism that can mediate the immune modulatory properties of cisplatin is the DNA sensing cGAS/STING pathway. The cGAS/STING interaction is not direct, via protein-protein interaction, but rather indirect, through the cyclic dinucleotide 2’3’-GMP-AMP (cGAMP), synthesized by cGAS from GTP and ATP. cGAMP acts as a second

messenger that directly binds to STING, leading to type I IFN production and downstream inflammation. While type I interferons are potent PD-L1 inducers, we could not detect IFNα or IFNβ secretion by tumor cells in response to cisplatin (data not shown). It is possible that additional tumor cell intrinsic mechanisms driven by oncogenes and /or tumors suppressors are mediating PD-L1 upregulation [31, 32]. Such mechanisms can also act alongside those triggered by adaptive immune resistance, secondary to T cell infiltration and IFNγ production [33]. Our results demonstrate that stimulation of the cGAS/STING pathway upregulates markers associated with immune recognition, providing the rationale to exploit this pathway for immune therapy. Intra-tumoral cGAMP administration in a few (non-ovarian) solid tumor models and B cell malignancies has demonstrated therapeutic efficacy [29, 34, 35]. Nevertheless, in addition to their anti-tumor roles, cGAS/STING and the associated inflammation can also carry pro-tumor functions that can influence tumors in various stages of development, from initiation to development and metastasis [36]. Recent data demonstrates that STING pathway can also trigger immune suppression, via interleukin- 10 (IL-10) and indoleamine 2,3-dioxygenase (IDO) [37, 38], pointing to the need for additional studies on cGAS/STING stimulation for therapeutic benefits.

The field of immuno-oncology has significantly expanded, mostly due to the success seen with anti-CTLA-4 and PD-1/PD-L1 blockade. Our studies show that single agent PD-L1 was efficient against aggressive tumors, although its efficacy was dependent on the tumor model. The less inflamed 2F8 responded better than the 2F8cis tumors, and the response was associated with CD8 infiltration and expression of IFNγ induced genes involved in antigen processing, MHC I presentation, and cytotoxic responses. Contrary to our expectation, the more inflamed 2F8cis tumors, which have increased mutational burden, heavier T cell infiltration, and presence of TLS, did not respond to single agent anti-PD-L1. This may be partly explained by the fact that 2F8cis tumors are more aggressive than 2F8 and that single agent treatment may have been started too late in our in vivo experiments. Nevertheless, the cisplatin/anti-PD-L1 combination increased survival in the aggressive, moderately cisplatin resistant model. Importantly, most of the DE genes triggered in the 2F8cis model were also associated with survival benefit in the 2F8 model, further reinforcing the significance of MHC I and genes associated with antigen processing and presentation as potential biomarkers of response to therapy.

In summary, our preclinical studies in two versatile mouse EOC models demonstrate that cisplatin modulates the immune environment, partly via the cGAS/STING pathway and that in combination with PD-1/PD-L1 blockade, it can increase survival in mice with aggressive tumors mirroring recurrent disease. Given the significant clinical response rates seen in patients treated with platinum compounds, we predict that chemotherapy will remain an important part of EOC standard of care. In light of the fact that emerging strategies targeting the immune system are becoming mainstream approaches for many solid tumor types, our data suggests that combination of cisplatin with immunotherapy may improve outcomes in future clinical trials, but an improved understanding of chemotherapy-induced immune modulation in EOC is clearly needed.

Materials and Methods

Cell lines

The 2F8 cell line was derived in house, from Cre-encoding adenovirus (AdCre)-induced orthotopic ovarian tumors [23, 24]. The primary tumor cells were cultured and cloned through limiting dilution, as previously described [23]. The 2F8 cells are p53 wild type and grow in vivo as high grade, undifferentiated epithelial tumors.

The 2F8cis cells were obtained by exposing the 2F8 cells in vitro to increasing concentrations of cisplatin (Sigma-Aldrich, St. Louis, MO), added continuously for more than 6 months. A continuous-exposure model was chosen [39], rather than a pulsed-exposure model. to ensure a more stable chemo resistant phenotype, with predictable in vitro and in vivo responses. Once stabilized at a level of moderate resistance, the 2F8cis cells have been maintained in culture by adding 1μM cisplatin to the culture medium. Both 2F8 and 2F8cis cells are grown in DMEM, complete with 4.5 g/L glucose, L-glutamine and sodium pyruvate, 1% penicillin/streptomycin, 1% non-essential amino acids (all from Corning Life Sciences, Corning, NY), 10% FBS (Atlanta Biologicals, Flowery Branch, GA), and 2-mercaptoethanol (Sigma-Aldrich). Human high grade serous ovarian cancer cell lines OVCA432 and OVCA420 were kindly provided by Dr. Olivera Finn (University of Pittsburgh, Pittsburgh, PA). Human cell lines were grown in complete RPMI (Corning Life Sciences).

In vitro treatment protocols and cell assays

All antibodies employed here (flow cytometry, IHC and immunoblot are listed in Suppl. Table 7). For the MTT assay, 2F8 and 2F8cis cells were plated at 3 000 cells per well and treated with cisplatin (Sigma) on day 2. Cisplatin was dissolved in PBS, diluted threefold to create an eight-point titration, and added to cells. Cell viability was measured with MTT cell proliferation kit (Trevigen, Gaithersburg, MD) after cisplatin treatment for 48 or 72 h. Cells were also treated with 2’3’-cGAMP (25 μg/mL), cisplatin at a pre-calculated IC50 concentration (determined by 72-hour MTT viability assay), or transfected with ISD/LyoVec™ and ISD Control/LyoVec™ (4 μg/mL) at different time periods. ISD/LyoVec™, Control/LyoVec™, 2’3’-cGAMP were purchased from InvivoGen (San Diego, CA).

For IFN stimulation, IFNα (Miltneyi Biotec) was added to culture at 10^4 IU/mL for 48 hours. For gene transfection experiments, the gene encoding for human cGAS (Genbank KC294566) and human STING (residues 335–1474, Genbank NM198282, joined via self-cleaving 2A peptide of porcine teschovirus-1 (GSGATNFSLLKQAGDVEENPGP), were synthesized (Genscript). 2A peptide was codon-optimized for optimal expression in mammalian cells using the UpGene codon optimization algorithm [40]. pAd/cGAS2ASTING was generated by subcloning the cGAS2ASTING gene into the shuttle vector, pAd (GenBank U62024) at *Sal* I/*Not* I sites. Subsequently, E1- ad E3-deleted replication-defective adenovirus 5, designated as Ad5.cGAS2ASTING, was generated by loxP homologous recombination on HEK-293 cells and purified by CsCl banding, followed by dialysis in 3% sucrose solution. Replication-defective adenovirus 5 expressing enhanced green fluorescence protein (Ad5.eGFP) was generated as previously described [41, 42].

Infectious titers were determined approximately 100-fold less than particle titers as previously described [43]. Viruses were aliquoted and stored at −80°C until use. Cells were infected with adenovirus at 2 000 MOI for 48 h, washed and then checked for efficiency of transfection via Western blot and flow cytometry.

Immunoblot

Cells were lysed in RIPA buffer plus Halt protease and phosphatase inhibitor cocktail (Thermo Scientific, Waltham, MA). Equal amounts of proteins were resolved on SDS-polyacrylamide gels and transferred to nitrocellulose membranes (Bio-Rad, Hercules, CA). After blocking with 5% blocking reagent, membranes were incubated with various primary antibodies (and appropriate secondary antibodies Suppl. Table 7). Images were acquired with an enhanced chemiluminescence system ECL (Thermo Scientific) and detected by ChemiDoc XRS system (Bio-Rad).

Flow cytometry

Fluorochrome - labelled monoclonal antibodies employed in flow cytometry (Suppl. Table 7) were used according to the manufacturer's protocol. For detection of calreticulin, a two-step staining protocol was used. Flow cytometric analysis was performed on an LSR II cytometer (BD Biosciences, Franklin Lakes, NJ) using FACSDiva (BD Biosciences) and FlowJo software (Tree Star, Ashland, OR). Based on the combined results from flow cytometry and immunoblots, we have characterized 2F8 and 2F8cis cells as relative to each other and are discussing them here as low and high, respectively, when describing cGAS, STING and PDL1 expression levels.

Immunohistochemistry (IHC)

Tumors from mouse necropsies were preserved in formalin prior to creating paraffin blocks. The local immune environment of tumors was evaluated with Foxp3, CD8, and PD-L1 antibodies following manufacturers' protocols. Details regarding antigen retrieval, primary and secondary (detection) antibodies are included in Suppl. Table 7.

Scoring of CD8 T cell infiltration was: 0 for < 5, 1 for < 15, 2 for <30 cells and 3 for ≥ 30 cells per high power field (hpf).

In vivo treatment protocols

All *in vivo* experiments were performed according to institutionally approved IACUC protocols. MUC1$^{+/-}$ Tg 129S1/SvlmJ 7–9 weeks old female mice were inoculated intraperitoneally (IP) with 2F8 cells (8×10^5) or 2F8cis cells (5×10^6) in 0.2 mL of PBS on Day 0. Pre-experimental testing had been done to determine an inoculation load sufficient to develop disease burden within a reasonable timeframe without overwhelming the animals and causing premature death. The need for a larger number of 2F8cis cells per inoculum is due to the inherent immunogenicity of this model. Animals were distributed in 4 treatment groups. No significant differences in mouse ages and weights were present. Mice were treated IP with either 200 μg anti-PD-L1 antibody (Suppl. Table 7), weight-based cisplatin (Sigma-Aldrich) or both drugs. Control mice received 200 μg rat IgG isotype control for anti-PD-L1 (Suppl. Table 7). Cisplatin dosage represented the mouse dose equivalent of

75mg/m^2 IP dose in humans. Mice received 3 treatments, every 2 weeks, starting 14 days after tumor challenge. For mice receiving combination therapy, IP cisplatin was given first, with anti-PD-L1 antibody administered IP the following day.

Mice were sacrificed three days following the last treatment or earlier, if moribund, as previously described [24]. Due to potential for "incomplete" take rate, following tumor challenge, mice with no evidence of disease at the end of protocol were excluded from the analysis. All removable tumor was dissected at necropsy and weighed for assessment of tumor burden. Sera from mice treated with cisplatin/anti-PD-L1 combination were tested for blood urea nitrogen and creatinine levels (Marshfield Laboratories, Marshfield, WI).

NanoString

RNA was isolated from tumors collected at necropsy and processed as per NanoString (Seattle, WA) guidelines and according to our previous protocols [23, 44]. We used the nCounter Mouse PanCancer Immune Profiling Panel kit containing probes for 751 immune genes.

RNA sequencing

Total RNA was extracted with the Qiagen AllPrep DNA/RNA Mini Kit (Hilden, Germany) and analyzed with Nanodrop spectrophotometer for concentration and purity. RNAseq was performed at the University of Pittsburgh Genomic Core using NextSeq 500/550 High Output 75 cycle kit (Illumina, San Diego, CA) with a single-read length and 40 million read depth.

Statistical analyses

Graphs and statistical calculations were generated using Prism 6 software (GraphPad, La Jolla, CA). The specific tests used to analyze each set of data are indicated in the figure legends. Appropriate tests were chosen based on whether the data follow a normal distribution. Statistical significance was assessed using a two-sided unpaired Student's *t* test to compare between two groups, one-way ANOVA to compare multiple groups, followed by the Tukey's *post-hoc* multiple comparisons test in case of statistically significant result, one-sample *t* test for fold change comparisons, log-rank (Mantel-Cox) test for the comparison of survival curves, and Fisher's exact test for assessment of TLS. In all cases, *P* values of < 0.05 were considered significant. Venn diagrams were generated using Venny 2.1 [45].

The raw RNAseq data were aligned to the reference genome (mm10 assembly) using TopHat2 aligner [46]. Bedtools was used to quantify and summarize read counts at the gene level [47]. Differentially expressed genes were identified with edgeR package in R [48]. Significance was determined using a likelihood ratio test and Benjamini-Hochberg correction for multiple comparisons. The MuTect algorithm was employed to identify somatic point mutations [49].

Supplementary Material

Refer to Web version on PubMed Central for supplementary material.

Acknowledgments

This study was partly supported by the NIH/NCI R01 CA163462, Pennsylvania Department of Health and a philanthropic donation from Mr. Matthew Fletcher Deitch.

References

1. Siegel RL, Miller KD, Jemal A. Cancer Statistics, 2017. CA Cancer J Clin 2017; 67: 7–30. [PubMed: 28055103]
2. Markman M, Bookman MA. Second-line treatment of ovarian cancer. Oncologist 2000; 5: 26–35. [PubMed: 10706647]
3. NCI. SEER Cancer Facts: Ovarian Cancer 2007–2013.
4. Le DT, Durham JN, Smith KN, Wang H, Bartlett BR, Aulakh LK et al. Mismatch-repair deficiency predicts response of solid tumors to PD-1 blockade. Science 2017.
5. McDermott DF, Drake CG, Sznol M, Choueiri TK, Powderly JD, Smith DC et al. Survival, Durable Response, and Long-Term Safety in Patients With Previously Treated Advanced Renal Cell Carcinoma Receiving Nivolumab. J Clin Oncol 2015; 33: 2013–2020. [PubMed: 25800770]
6. Reck M, Rodriguez-Abreu D, Robinson AG, Hui R, Csoszi T, Fulop A et al. Pembrolizumab versus Chemotherapy for PD-L1-Positive Non-Small-Cell Lung Cancer. N Engl J Med 2016; 375: 1823–1833. [PubMed: 27718847]
7. Topalian SL, Sznol M, McDermott DF, Kluger HM, Carvajal RD, Sharfman WH et al. Survival, durable tumor remission, and long-term safety in patients with advanced melanoma receiving nivolumab. J Clin Oncol 2014; 32: 1020–1030. [PubMed: 24590637]
8. Gaillard SL, Secord AA, Monk B. The role of immune checkpoint inhibition in the treatment of ovarian cancer. Gynecol Oncol Res Pract 2016; 3: 11. [PubMed: 27904752]
9. Topalian SL, Drake CG, Pardoll DM. Immune checkpoint blockade: a common denominator approach to cancer therapy. Cancer Cell 2015; 27: 450–461. [PubMed: 25858804]
10. Hamanishi J, Mandai M, Iwasaki M, Okazaki T, Tanaka Y, Yamaguchi K et al. Programmed cell death 1 ligand 1 and tumor-infiltrating CD8+ T lymphocytes are prognostic factors of human ovarian cancer. Proc Natl Acad Sci U S A 2007; 104: 3360–3365. [PubMed: 17360651]
11. Hamanishi J, Mandai M, Ikeda T, Minami M, Kawaguchi A, Murayama T et al. Safety and Antitumor Activity of Anti-PD-1 Antibody, Nivolumab, in Patients With Platinum-Resistant Ovarian Cancer. J Clin Oncol 2015; 33: 4015–4022. [PubMed: 26351349]
12. Varga AP-PS, Ott PA, Mehnert JM, Berton-Rigaud D, Morosky A. Pembrolizumab in patients (pts) with PD-L1–positive (PD-L1+) advanced ovarian cancer: Updated analysis of KEYNOTE-028. Journal of Clinical Oncology 2017; 35: 5513–5513.
13. Disis ML PM, Pant S, Hamilton EP, Lockhart AC, Kelly K. Avelumab (MSB0010718C; anti-PD-L1) in patients with recurrent/refractory ovarian cancer from the JAVELIN Solid Tumor phase Ib trial: Safety and clinical activity. Journal of Clinical Oncology 2016; 34: 5533–5533.
14. Hamanishi J, Mandai M, Konishi I. Immune checkpoint inhibition in ovarian cancer. Int Immunol 2016; 28: 339–348. [PubMed: 27055470]
15. Sharma P, Hu-Lieskovan S, Wargo JA, Ribas A. Primary, Adaptive, and Acquired Resistance to Cancer Immunotherapy. Cell 2017; 168: 707–723. [PubMed: 28187290]
16. Dasari S, Tchounwou PB. Cisplatin in cancer therapy: molecular mechanisms of action. Eur J Pharmacol 2014; 740: 364–378. [PubMed: 25058905]
17. Beyranvand Nejad E, van der Sluis TC, van Duikeren S, Yagita H, Janssen GM, van Veelen PA et al. Tumor Eradication by Cisplatin Is Sustained by CD80/86-Mediated Costimulation of CD8+ T Cells. Cancer Res 2016; 76: 6017–6029. [PubMed: 27569212]
18. Di Blasio S, Wortel IM, van Bladel DA, de Vries LE, Duiveman-de Boer T, Worah K et al. Human CD1c(+) DCs are critical cellular mediators of immune responses induced by immunogenic cell death. Oncoimmunology 2016; 5: e1192739. [PubMed: 27622063]
19. Merritt RE, Mahtabifard A, Yamada RE, Crystal RG, Korst RJ. Cisplatin augments cytotoxic T-lymphocyte-mediated antitumor immunity in poorly immunogenic murine lung cancer. J Thorac Cardiovasc Surg 2003; 126: 1609–1617. [PubMed: 14666041]

20. Mesnage SJL, Auguste A, Genestie C, Dunant A, Pain E, Drusch F et al. Neoadjuvant chemotherapy (NACT) increases immune infiltration and programmed death-ligand 1 (PD-L1) expression in epithelial ovarian cancer (EOC). Ann Oncol 2017; 28: 651–657. [PubMed: 27864219]
21. Bast RC, Jr., Feeney M, Lazarus H, Nadler LM, Colvin RB, Knapp RC. Reactivity of a monoclonal antibody with human ovarian carcinoma. J Clin Invest 1981; 68: 1331–1337. [PubMed: 7028788]
22. Havrilesky LJ, Elbendary A, Hurteau JA, Whitaker RS, Rodriguez GC, Berchuck A. Chemotherapy-induced apoptosis in epithelial ovarian cancers. Obstet Gynecol 1995; 85: 1007–1010. [PubMed: 7770245]
23. Mony JT, Zhang L, Ma T, Grabosch S, Tirodkar TS, Brozick J et al. Anti-PD-L1 prolongs survival and triggers T cell but not humoral anti-tumor immune responses in a human MUC1-expressing preclinical ovarian cancer model. Cancer Immunol Immunother 2015; 64: 1095–1108. [PubMed: 25998800]
24. Budiu RA, Elishaev E, Brozick J, Lee M, Edwards RP, Kalinski P et al. Immunobiology of human mucin 1 in a preclinical ovarian tumor model. Oncogene 2013; 32: 3664–3675. [PubMed: 22964632]
25. Dieu-Nosjean MC, Goc J, Giraldo NA, Sautes-Fridman C, Fridman WH. Tertiary lymphoid structures in cancer and beyond. Trends Immunol 2014; 35: 571–580. [PubMed: 25443495]
26. Taube JM, Klein A, Brahmer JR, Xu H, Pan X, Kim JH et al. Association of PD-1, PD-1 ligands, and other features of the tumor immune microenvironment with response to anti-PD-1 therapy. Clin Cancer Res 2014; 20: 5064–5074. [PubMed: 24714771]
27. Garcia-Diaz A, Shin DS, Moreno BH, Saco J, Escuin-Ordinas H, Rodriguez GA et al. Interferon Receptor Signaling Pathways Regulating PD-L1 and PD-L2 Expression. Cell Rep 2017; 19: 1189–1201. [PubMed: 28494868]
28. Parker BS, Rautela J, Hertzog PJ. Antitumour actions of interferons: implications for cancer therapy. Nat Rev Cancer 2016; 16: 131–144. [PubMed: 26911188]
29. Feng M, Chen JY, Weissman-Tsukamoto R, Volkmer JP, Ho PY, McKenna KM et al. Macrophages eat cancer cells using their own calreticulin as a guide: roles of TLR and Btk. Proc Natl Acad Sci U S A 2015; 112: 2145–2150. [PubMed: 25646432]
30. Yang H, Wang H, Ren J, Chen Q, Chen ZJ. cGAS is essential for cellular senescence. Proceedings of the National Academy of Sciences 2017; 114: E4612–E4620.
31. Cortez MA, Ivan C, Valdecanas D, Wang X, Peltier HJ, Ye Y et al. PDL1 Regulation by p53 via miR-34. J Natl Cancer Inst 2016; 108.
32. Hughes PE, Caenepeel S, Wu LC. Targeted Therapy and Checkpoint Immunotherapy Combinations for the Treatment of Cancer. Trends Immunol 2016; 37: 462–476. [PubMed: 27216414]
33. Webb JR, Milne K, Kroeger DR, Nelson BH. PD-L1 expression is associated with tumor-infiltrating T cells and favorable prognosis in high-grade serous ovarian cancer. Gynecol Oncol 2016; 141: 293–302. [PubMed: 26972336]
34. Demaria O, De Gassart A, Coso S, Gestermann N, Di Domizio J, Flatz L et al. STING activation of tumor endothelial cells initiates spontaneous and therapeutic antitumor immunity. Proceedings of the National Academy of Sciences of the United States of America 2015; 112: 15408–15413. [PubMed: 26607445]
35. Tang CH, Zundell JA, Ranatunga S, Lin C, Nefedova Y, Del Valle JR et al. Agonist-Mediated Activation of STING Induces Apoptosis in Malignant B Cells. Cancer research 2016; 76: 2137–2152. [PubMed: 26951929]
36. Bakhoum SF, Ngo B, Laughney AM, Cavallo JA, Murphy CJ, Ly P et al. Chromosomal instability drives metastasis through a cytosolic DNA response. Nature 2018; 553: 467–472. [PubMed: 29342134]
37. Lemos H, Mohamed E, Huang L, Ou R, Pacholczyk G, Arbab AS et al. STING Promotes the Growth of Tumors Characterized by Low Antigenicity via IDO Activation. Cancer research 2016; 76: 2076–2081. [PubMed: 26964621]

38. Liang D, Xiao-Feng H, Guan-Jun D, Er-Ling H, Sheng C, Ting-Ting W et al. Activated STING enhances Tregs infiltration in the HPV-related carcinogenesis of tongue squamous cells via the c-jun/CCL22 signal. Biochimica et biophysica acta 2015; 1852: 2494–2503. [PubMed: 26303640]
39. Jiang RD, Zhang LX, Yue W, Zhu YF, Lu HJ, Liu X et al. [Establishment of a human nasopharyngeal carcinoma drug-resistant cell line CNE2/DDP and screening of drug-resistant genes]. Ai Zheng 2003; 22: 337–345. [PubMed: 12703984]
40. Gao W, Rzewski A, Sun H, Robbins PD, Gambotto A. UpGene: Application of a web-based DNA codon optimization algorithm. Biotechnol Prog 2004; 20: 443–448. [PubMed: 15058988]
41. Feili-Hariri M, Falkner DH, Gambotto A, Papworth GD, Watkins SC, Robbins PD et al. Dendritic cells transduced to express interleukin-4 prevent diabetes in nonobese diabetic mice with advanced insulitis. Hum Gene Ther 2003; 14: 13–23. [PubMed: 12573055]
42. Hardy S, Kitamura M, Harris-Stansil T, Dai Y, Phipps ML. Construction of adenovirus vectors through Cre-lox recombination. J Virol 1997; 71: 1842–1849. [PubMed: 9032314]
43. Bilbao R, Reay DP, Hughes T, Biermann V, Volpers C, Goldberg L et al. Fetal muscle gene transfer is not enhanced by an RGD capsid modification to high-capacity adenoviral vectors. Gene Ther 2003; 10: 1821–1829. [PubMed: 12960972]
44. Grabosch S, Tseng G, Edwards RP, Lankes HA, Moore K, Odunsi K et al. Multiplex profiling identifies distinct local and systemic alterations during intraperitoneal chemotherapy for ovarian cancer: An NRG Oncology/Gynecologic Oncology Group Study. Gynecol Oncol 2017.
45. Oliveros JC. An interactive tool for comparing lists with Venn's diagrams. 2007–2015.
46. Kim D, Pertea G, Trapnell C, Pimentel H, Kelley R, Salzberg SL. TopHat2: accurate alignment of transcriptomes in the presence of insertions, deletions and gene fusions. Genome Biol 2013; 14: R36. [PubMed: 23618408]
47. Quinlan AR, Hall IM. BEDTools: a flexible suite of utilities for comparing genomic features. Bioinformatics 2010; 26: 841–842. [PubMed: 20110278]
48. Robinson MD, McCarthy DJ, Smyth GK. edgeR: a Bioconductor package for differential expression analysis of digital gene expression data. Bioinformatics 2010; 26: 139–140. [PubMed: 19910308]
49. Cibulskis K, Lawrence MS, Carter SL, Sivachenko A, Jaffe D, Sougnez C et al. Sensitive detection of somatic point mutations in impure and heterogeneous cancer samples. Nat Biotechnol 2013; 31: 213–219. [PubMed: 23396013]

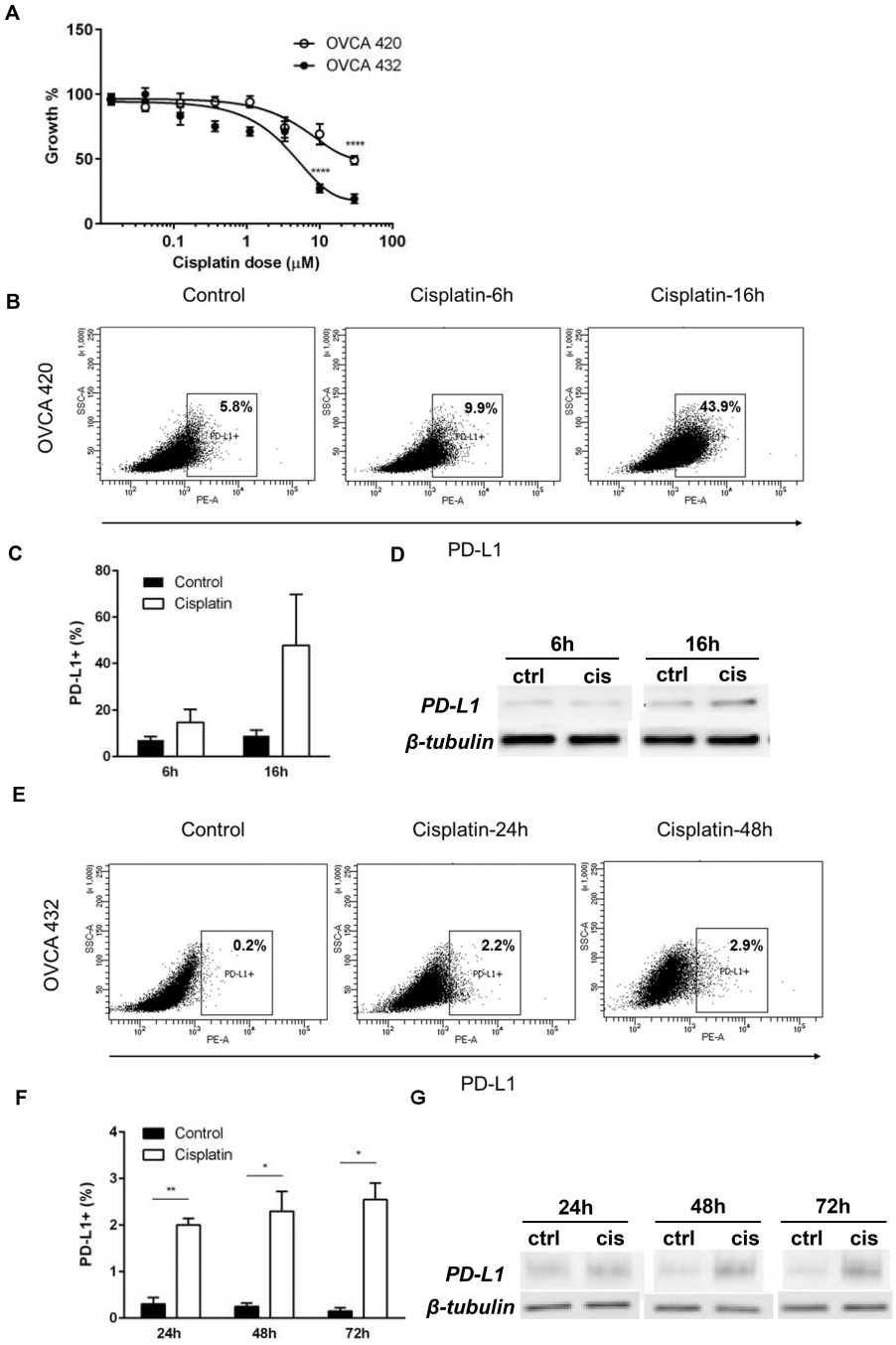

Fig. 1.

(A) Cisplatin dose response growth curves of OVCA432 (open circles) and OVCA420 human EOC cells (black circles). Measurements at 48 h were obtained via MTT assay and were performed in triplicate. SD bars are shown (**** $p<0.0001$, Student t test.) (B, E) PD-L1 expression in OVCA420 and OVCA432 cells (B and E, respectively), treated with cisplatin IC50 at various time points.Gates were set according to isotype control . (C, F) Percentages of PD-L1 positive OVCA420 (C) and OVCA432 (F) cells in culture, in the absence (control) or presence of IC50 cisplatin, at various time points. Averages of

percentages from two separate experiments are shown. (D, G) PD-L1 detection in cell lysates from OVCA420 (D) and OVCA432 cells (G), by Western blot. Cells were treated with IC50 cisplatin, for the time shown. Beta-tubulin was used as loading control.

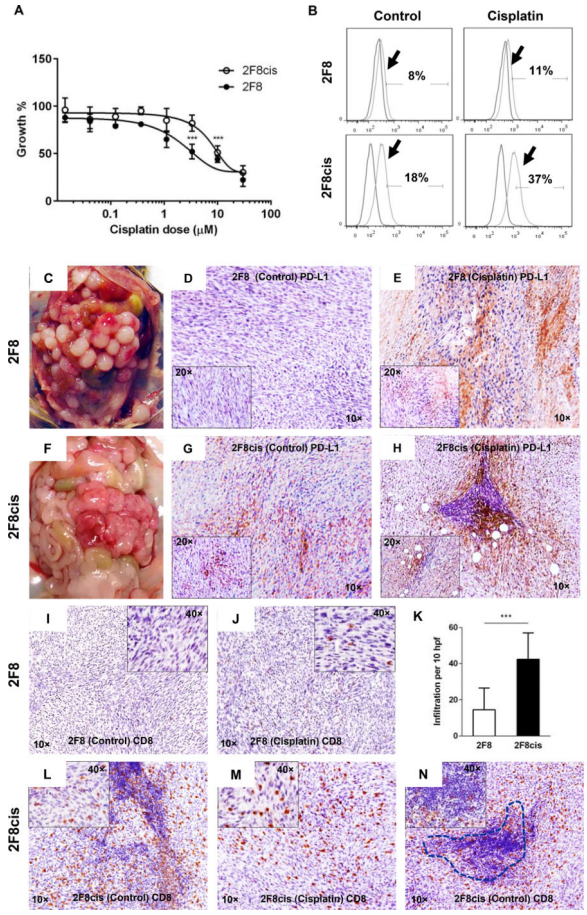

Fig. 2.

(A) Dose response curves of mouse 2F8 (black circles) and 2F8cis cells (open circles) treated with cisplatin for 48 h. (B) Flow cytometry showing histograms for PD-L1 expression (arrows) in 2F8 (top) and 2F8cis cells (bottom). Isotype control curves were used for gating. Percentages represent PDL1 positive cells. (C, F) Intraperitoneal tumor challenge with 2F8 (C) and 2F8cis cells (F) leads to extensive peritoneal carcinomatosis. (D, G, E, H) Tissue PD-L1 expression detected by IHC in untreated 2F8 (D) and 2F8cis tumors (G) and after cisplatin treatment (E and H, respectively). Images were acquired at 10x; insets in D and E represent images at 20x. (I-N) IHC dentification of CD8 T cells in 2F8 (I, J) and 2F8cis tumors (L-N) via IHC, before (I, L) and after cisplatin treatment (J, M). (K) Average CD8 T cell counts per 10 high power fields (hpf) and SD, in 2F8 and 2F8cis tumors. $P<0.001$ Student t test. (N) CD8 T cells inside the tumor mass and within a tertiary lymphoid-like structure (dotted line) in a representative 2F8cis tumor.

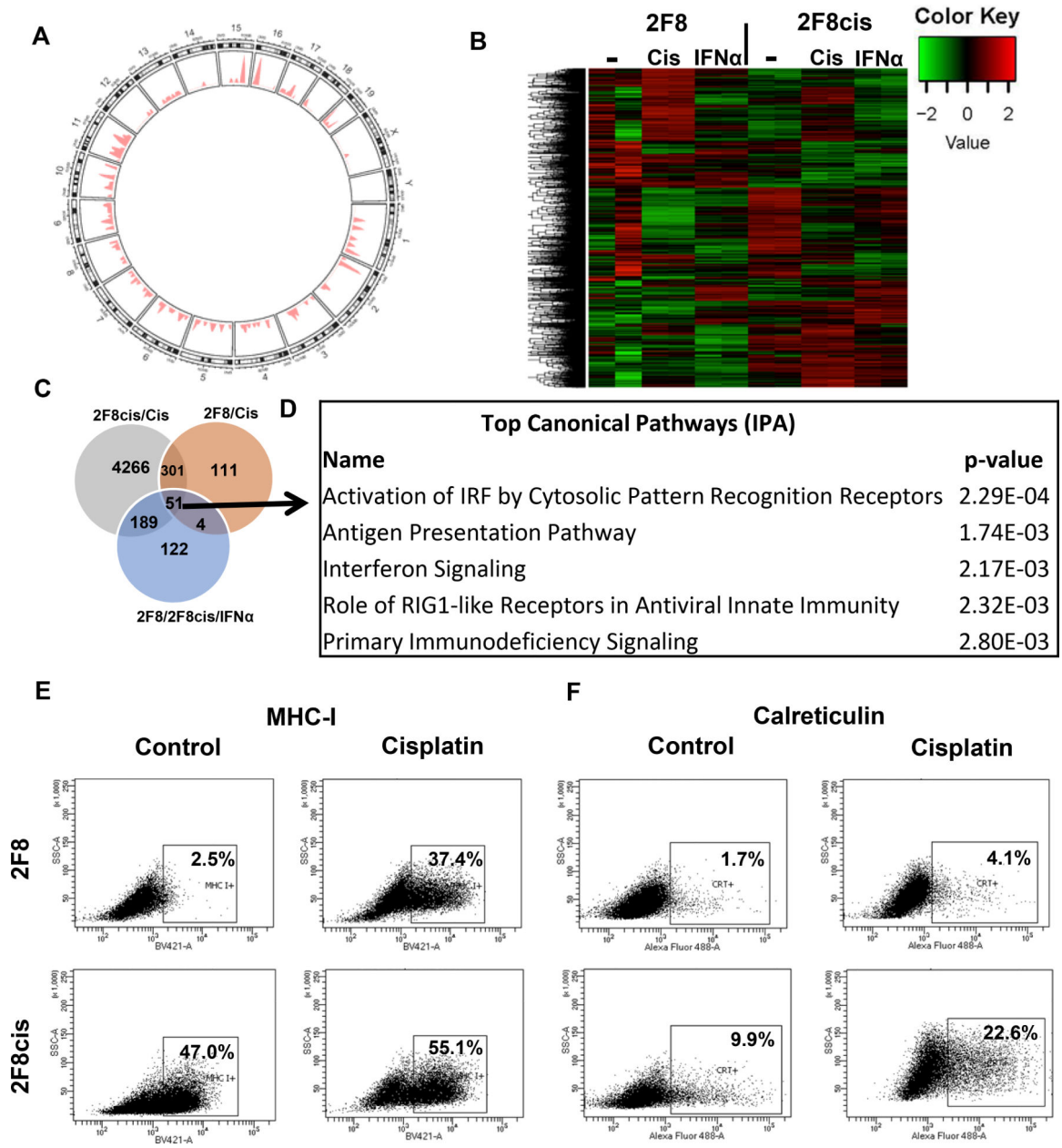

Fig. 3.

(A) Somatic point mutations (n=202) identified in 2F8cis cells, using 2F8 cells as reference. The genome-wide distribution of mutations is shown in a circos plot. The chromosomes are numbered and arranged in a circular orientation. The x-axis corresponds to the genomic regions by chromosome, the y-axis corresponds to the density/frequency of mutations in each chromosome. (B) Heat map of DE genes (n= 4074 selected genes, with greater than Q3 expression level and greater than Q3 variance) in 2F8 and 2F8cis cells, either untreated (−), exposed to cisplatin (cis) or IFNα. Samples were run in duplicate. (C) Venn diagram of DE genes. Grey circle represents DE genes upregulated by cisplatin treatment in 2F8cis cells compared to control treated. Brown circle represents the DE genes upregulated by cisplatin treatment in 2F8 cells, compared to control cells. Light blue circle represents DE genes

commonly upregulated by IFNα in both 2F8 and 2F8cis cells.All genes are listed in Supplementary Table 2 ($q<0.05$) (D) Top 5 pathways identified via Ingenuity Pathway Analysis, using the common DE genes from the three-circle intersection (n=51 genes, listed in Suppl. Table 2). (E, F) MHC I (E) and calreticulin (F) detection via flow cytometry of 2F8 (top) and 2F8cis cells (bottom), either untreated (ctr) or exposed to IC50 cisplatin for 48 h. Percentages represent positive cells, using isotype control for gating. Results of at least three independent experiments are shown.

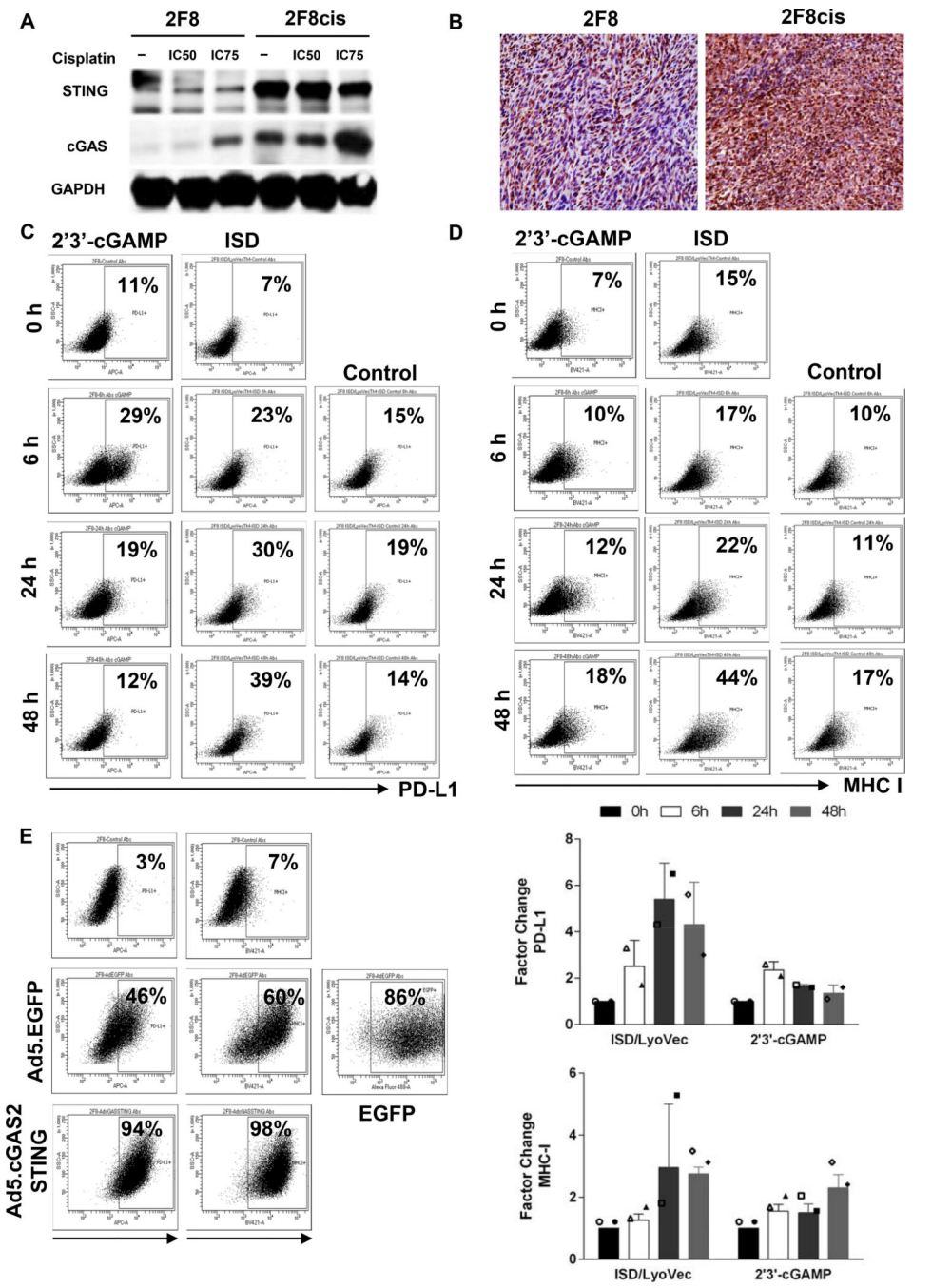

Fig. 4.

(A) Detection of cGAS and STING proteins by Western blot, using lysates from 2F8 and 2F8cis cells either untreated (−) or exposed to IC50 and IC75 cisplatin. GAPDH was used as loading control. (B) Detection of STING protein by IHC, in 2F8 (left) and 2F8cis tumors (right). (C, D) PD-L1 (C) and MHC I (D) detected by flow cytometry, following exposure of 2F8 cells to STING ligand 2'3'-cGAMP and ISD oligomer. Control indicates treatment with a non-immunostimulatory single-stranded oligonucleotide. (E) PD-L1 and MHC I expression detected by flow cytometry in 2F8 cells transduced with adenovirus encoding for

cGAS/STING (Ad5.cGAS2ASTING) for 48 hours. Untreated and control adenovirus (Ad5.EGFP) treated cells are shown as reference. Percentages represent positive cells. Gates were set up based on staining with isotype control antibodies for each respective marker. EGFP positive cells indicate transfection efficiency. (F). Average expression of PD-L1(top) and MHC I (bottom) detected by flow cytometry in 2F8 cells following exposure to STING ligand 2'3'-cGAMP and ISD oligomer. Factor change represents the ratio of percent positive cells in the treatment group to control.The symbols represent measurements from separate experiments.

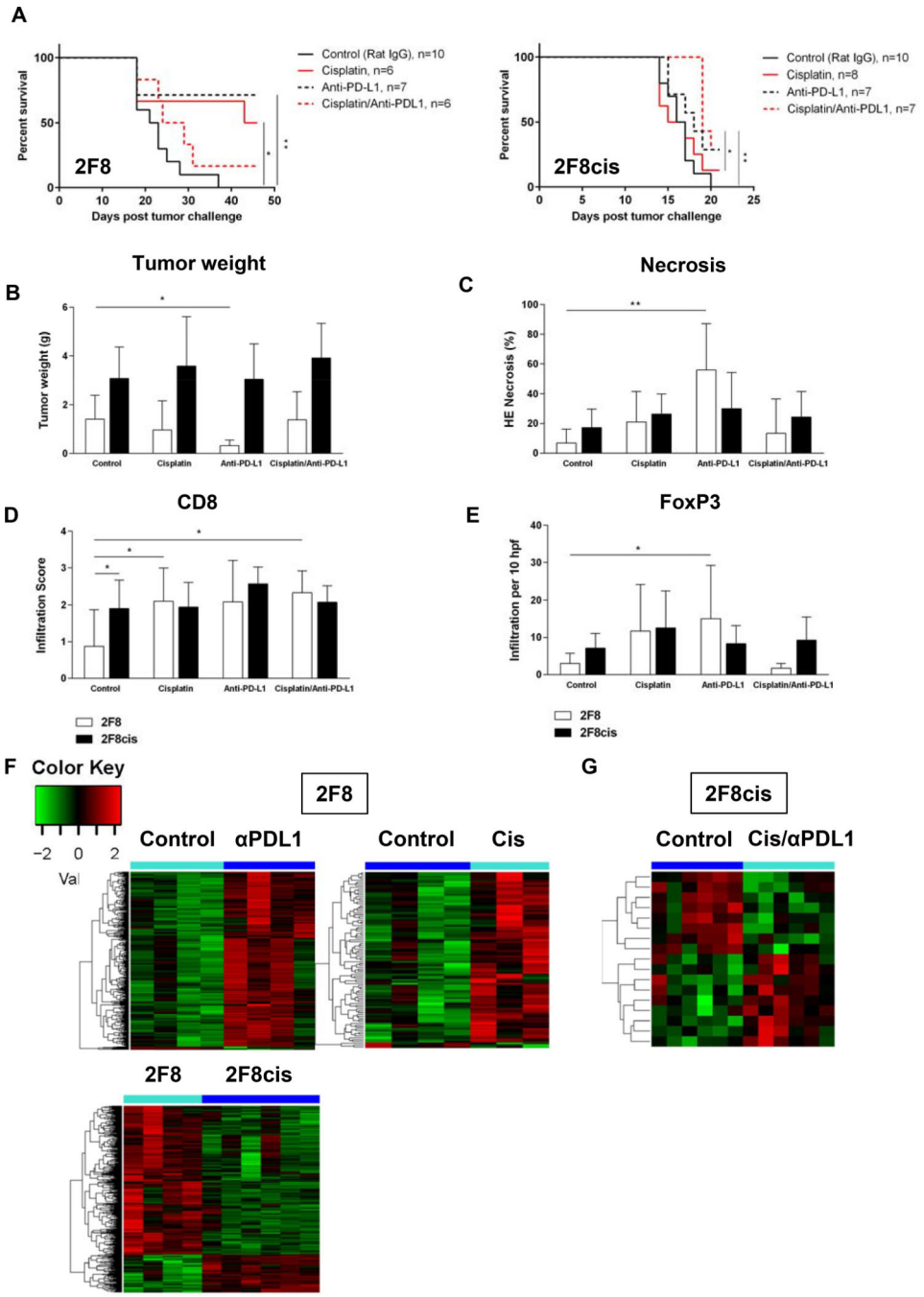

Fig. 5.

(A) Kaplan-Meier survival curves of mice injected IP with either 2F8 cells (left) or 2F8cis cells (right) and treated with either control antibody (solid black line), cisplatin (solid red line), anti-PD-L1- (dotted black line) or cisplatin/anti-PD-L1 combination (dotted red line). * $p<0.05$; ** $p<0.005$ (log-rank test). (B-E) Changes in tumor burden (B) necrosis areas (C), CD8 (D) and Foxp3 T cell infiltration (E) in mice with 2F8 (grey bars) and 2F8cis tumors (black bars). * $p<0.05$ Student t test. Average values for the group and SD are shown. (F, G) Heatmap of DE genes triggered by survival-increasing treatments in the 2F8 (F) and 2F8cis

model (G). Up- and down-regulated genes are shown red and green, respectively. All genes shown in the heatmaps are listed in Suppl. Table 4. (H) Heatmap of DE genes in 2F8cis compared to 2F8 tumors. Genes are listed in Suppl. Table 6. All heatmaps use the scale shown in panel F.